**RESEARCH ARTICLE**

# Frequency Control of Low Inertia Power Grids With Fuel Cell Systems in Distribution Networks

**ABOUZAR ESTEBSARI**[1], (Senior Member, IEEE), **STEFFEN VOGEL**[2], (Student Member, IEEE),
**RENATO MELLONI**[2,3], **MARIJA STEVIC**[2,4], **ETTORE F. BOMPARD**[3], (Member, IEEE),
**AND ANTONELLO MONTI**[2], (Senior Member, IEEE)

[1]School of the Built Environment and Architecture, London South Bank University, London SE1 0AA, U.K.
[2]Institute for Automation of Complex Power Systems, RWTH Aachen University, 52074 Aachen, Germany
[3]Department of Energy, Politecnico di Torino, 10129 Turin, Italy
[4]OPAL-RT Germany GmbH, 90408 Nuremberg, Germany

Corresponding author: Abouzar Estebsari (estebsaa@lsbu.ac.uk)

**ABSTRACT** High penetration of variable renewable energy resources to distribution networks brings new challenges to frequency control in transmission systems; notwithstanding, coordinated exploitation of some widely distributed resources in distribution networks could support overall system frequency control. We developed a centralized control scheme to utilize existing solid oxide fuel cell systems in distribution networks to mitigate frequency deviation in the transmission system. This novel control scheme minimizes curtailing renewable resources. It appropriately prioritizes adjusting active or reactive power of medium voltage connected fuel cell systems to efficiently provides frequency support, while keeping the renewable sources connected. A co-simulation platform was also developed to allow for analyzing the interactions between transmission and distribution networks. It enhances simulation capability through parallel distributed real-time simulations. This platform enables ex-ante analysis of the impact of control strategies of distribution system on transmission system. A set of experimental results on European transmission and distribution network benchmarks demonstrated the performance of the developed primary frequency control scheme using solid oxide fuel cell systems.

**INDEX TERMS** Frequency control, fuel cells, power distribution, power transmission, simulation.

## I. INTRODUCTION

Nowadays, distribution networks (DN) are changing rapidly due to high penetration of distributed energy resources (DER), energy storage systems (ESSs) and controllable loads. Integration of these new technologies to DNs poses a lot of challenges to the planning and operation of electrical power systems. Whilst on one hand DERs can threaten the overall reliability of the electrical power system, on the other hand they could also have a positive effect if used properly for network support [1]–[3]. For instance, in [4] a centralized reactive power management strategy for PV systems is proposed. It aims to reduce system's losses by using the capability of grid-connected PV inverter to provide reactive power.

The associate editor coordinating the review of this manuscript and approving it for publication was Jahangir Hossain.

In case of absence or very low penetration of DERs, network normal operation and stability is less jeopardized since the protection of local resources is conventionally achieved by curtailing DERs under any abnormal conditions (e.g. voltage drops or frequency deviation). Recent national grid codes define advanced requirements for DER functions, including active and reactive power control, voltage and frequency support, and fault ride-through (FRT) capability.

The above-mentioned considerations lead to the need of integrated simulations of transmission and distribution networks, both represented with their corresponding detailed models [5]. Such simulations allow investigation of the impact of DERs, installed in DNs, on the transmission network (TS) and their prospective support for system stability and reliability. Combined simulation and analysis of interactions between TN-DN is nowadays an emerging research

topic. Some projects focus on specific occurrences and do not use complete joint simulations for TN and DN [6]–[9], while others introduce co-simulation platforms that can be used for studying the modern power system [10], [11].

In the context of TN-DN co-simulations, we developed a new co-simulation platform by interfacing two digital real-time simulators (DRTS) from RTDS and OPAL-RT Technologies. This platform not only ensures general benefits of performing real-time simulations (e.g. software in-the-loop and hardware in-the-loop), but also improves overall computation power by clustering several digital simulators from different providers. Coupling the simulators via field programmable gate arrays (FPGAs) and fiber optics allows for a synchronized and a fully digital interface which eliminates analog conversion errors and reduces end-to-end latency between the simulators to few time-steps.

Besides setting up this co-simulation platform, we implemented some benchmark models of TN and DN with detailed models of some DERs such as Fuel Cell and PV systems for real-time simulation, and designed DN equivalents for realistic and scalable interaction studies. These efforts would greatly contribute in studying the impacts of widely distributed energy recourse of DN on TN, and the role they can play in supporting system frequency or voltage regulation.

The widespread of DERs is rapidly leading to new business opportunities, different market models and new alternatives for ancillary services. For this reason, in [12] the electrical system is examined with a wider approach, including commercial aspects (day ahead commitment, real-time dispatch, etc.). In [13] TSOs and DSOs are involved in the project in order to have a complete framework from each point of view.

In scope of the analysis of TN-DN interactions, we focus on the contribution of dispersed solid oxide fuel cell (SOFC) systems along with existing PV generation in DNs to frequency regulation.

Besides their potential use for virtual inertia, battery energy storage systems (BESSs) are perfectly suitable for participating in primary and secondary frequency regulation, at least from a technical point of view. The biggest concern about the use of BESSs for frequency control is the economic feasibility. Participation in primary or secondary control, stand-alone installation or supporting a non-programmable power plant, strongly affect revenues and lifetime. Also, the local market influences the economic feasibility: according to [14] and [15] in Italy it is more convenient to participate in secondary regulation, while in Denmark the most convenient application for batteries is the primary regulation.

Likewise, with batteries, fuel cell (FC) power plants can participate in primary frequency control. The type of fuel processor used for providing the hydrogen-rich fuel to FC stacks depends on the technology used for the fuel cell. The former is often the main limit to the dynamic performances of this kind of power plant. However, the use of certain types of FC stacks and/or the presence of hydrogen storage, allow participating in primary frequency control. FC stacks are of particular interest for the grid support due to their independency from weather conditions, fast response when fuel supplied from hydrogen storage and flexibility in terms of hydrogen supply.

In [16] a good example of the contribution of combination of fuel cells and wind turbines is presented for providing inertial and primary frequency regulation.

By reviewing literature, in general the contribution of fuel cells in frequency control is found to be more either on frequency regulation in standalone microgrids or islanded grids [17]–[19], or controlling fuel cell inverters to ensure output power with set-point/reference frequency [19]–[21].

Frequency regulation by fuel cells is found to be more decentralized through local control systems. In this paper, we present our developed centralized control strategy to coordinate the fuel cell systems in the distribution networks with high penetration of DER (e.g. PV) to provide support for frequency regulation in transmission network. This control system applies a priority-based strategy to manage generation of active and reactive power by distributed fuel cells in distribution network, eventually providing frequency support directly by control of active power and indirectly by control of reactive power.

Control of active power of SOFC could directly support frequency regulation by prompt response of SOFCs in terms of increasing or decreasing output active power. However, neglecting the impact of critical conditions on the voltage level of the nodes with DERs could result in DER curtailment. Curtailing some DERs due to voltage drop would diminish or even deactivate SOFCs' frequency support. Therefore, only controlling active power of SOFCs is not sufficient and controlling reactive power to support voltage regulation is also required not to lose other DERs.

The DERs with high penetration in our study are PV generators with regulated low voltage ride-through (LVRT) capability. The studies include intermittent behavior of distributed PV systems under critical conditions, such as sudden change in weather conditions. SOFC systems can be used to support the primary frequency response of the electrical power system also if the DNs which accommodate them withstand some level of voltage at the connection points of PVs. Contribution of SOFC to voltage regulation allows PV generators to remain connected and thus indirectly support mitigation of frequency deviation.

In this paper, different control strategies are proposed to use the capability of power electronic inverters which connect SOFCs to the network. The voltage support through reactive power injection is included in the investigation and the strategies are tested in laboratory experiments.

The evaluation of system frequency response is also made using different strategies for FCs frequency controller and it is based on frequency metrics for variable renewable generation proposed by LBNL [22].

We also developed a co-simulation platform based on digital real-time simulators to overcome the challenge of computation demand of analyzing interplays in large scale network. Coupling digital real-time simulators enables the

simulation of more complex scenarios by combining modelling tools and/or existing models of different vendors. The new interface allows for deterministic and error-free exchange of analog interface signals by using a fully digital path between the simulators. This eliminates jitter and quantization errors introduced by traditional analog HIL interfaces.

In the next section, Section II, contribution of FC in power system frequency regulation is discussed with introducing the FC model and local controller we implemented as well as frequency performance metrics. Section III introduces the platform designed for real-time co-simulation of transmission-distribution networks, and in Section IV the developed centralized control strategy to coordinate FCs is introduced and its performance is assessed by some simulation results in Section V. Finally, Section VI presents some conclusions and remarks.

## II. FUEL CELL SYSTEM CONTRIBUTION TO FREQUENCY REGULATION

Thanks to large bulk generators in traditional power systems, frequency response of the system is well controlled and optimized. But todays, the spread of RESs (Renewable Energy Resources), distributed generators and the use of HVDC for interconnection, introduce new concerns about frequency security and reliability. Distributed, and often non-dispatchable, generators are increasingly replacing traditional large and well controllable power plants resulting in a lack of inertia from rotating machines. Furthermore, performances of primary frequency control strongly depend on the total nominal power of (synchronous) generators participating in primary regulation, which is reducing.

Since the minimum frequency value reached during a frequency transient mainly depends on system inertia, a system with a low kinetic energy level is more vulnerable to power imbalance event. In the isolated power systems, two main factors make the system particularly more vulnerable to generation outages: the size of the system which is quite small with a low inertia level, and the low number of available large generators which provide power.

Besides issues and concerns, changing paradigm of electrical networks can bring new opportunities and solutions for frequency control [23], [24]. Distributed generation, controllable loads and energy storage systems can support the electrical system in every frequency-related aspect, from inertial response to power reserves for frequency control. This is possible thanks to new technologies and coordination among components and actors involved in grid operations.

In this context, we focus on participation of existing solid oxide fuel cells in primary frequency control and their impact on the overall frequency response. As already mentioned, the advantage of SOFC systems compared to solar or wind energy sources is their independency from weather conditions and fast response when fuel supplied from hydrogen storage. This overcomes reliability issues that would arise if the frequency regulation was partly provided, for instance, by PV systems. Before discussing the effectiveness of fuel cell's

contribution in frequency regulation, first we shortly present the fuel cell models and controller which we implemented, and then we introduce performance indices for examining the primary frequency control.

### A. FUEL CELL SYSTEM MODEL

Solid Oxide Fuel Cell (SOFC) systems are widely used in stationary applications because of their high efficiency. Thanks to the high operating temperature of SOFCs, which is around $1000°C$, CO and hydrocarbons (e.g. CH4) can be internally converted to hydrogen [25], [26]. Therefore, the input of SOFCs is not necessarily pure hydrogen [27]. The FC model implemented in MATLAB/Simulink is based on [28]–[30]. It is implemented in the controller of a negative controllable load block of the Simulink library and contains the following assumptions:

–Gases are real,

–Fixed temperature at all times,

–Nernst equation can be applied,

–The channels, which transport gases, have a fixed value but a small length: it is enough to define one pressure inside the channel,

–Time response of the power converter is much faster than that of the fuel cell system. For this reason, the dynamics of a power converter has been neglected,

–The exhaust of each channel is via a single orifice and the ratio of internal and external pressures is large enough to consider that the orifice is choked.

The SOFC system model consists two main parts: the so-called balance of plant (BOP) and the fuel cell stack.

In the BOP, high-pressure fuel is delivered to the reformer by controlling a valve. Here, the fuel is converted into hydrogen-rich fuel and delivered to fuel cell stack. Reformer's dynamic affects strongly the overall performance of the system.

In SOFC stacks, the electrode reaction that occurs is shown by (1). At the anode, oxygen ions react with hydrogen, and water vapor besides is formed. Electrical energy is released in form of electrons. At the cathode, electrons taken from the anode react with oxygen.

$$Anode : H_2 + O^= \rightarrow H_2O + 2e^-$$
$$Cathode : \frac{1}{2}O_2 + 2e^- \rightarrow O^= \tag{1}$$
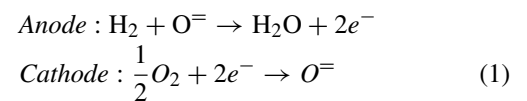
When a mixture of gases of average molar mass, $M$ [kg/mol] and similar specific heat ratios passes through an orifice that can be considered choked at a constant temperature, the following characteristic is met:

$$\frac{W}{P_u} = K \cdot \sqrt{M} \tag{2}$$

where $W$ is the mass flow [kg/s]; $K$ is the valve constant and depends mainly on the area of the orifice [$\sqrt{\mathrm{kmolkg}}/(\mathrm{atm\ s})$] and $P_u$ is the pressure inside the channel [atm]. Fuel utilization factor ($u$) is the ratio between the fuel flow that reacts and the fuel flow injected to the stack and it is a way to express

the water molar fraction at the exhaust. Therefore, (2) for the anode can be written as:

$$\frac{W_{an}}{P_{an}} = K_{an} \cdot \sqrt{(1-u) \cdot M_{H_2} + u \cdot M_{H_2O}} \qquad (3)$$

where *an* indicates quantities regarding the anode. If the molar flow of a gas through the valve can be considered proportional to its partial pressure inside the channel, (5) is derived from expressions (4).

$$\frac{N_{H_2}}{p_{H_2}} = \frac{K_{an}}{\sqrt{M_{H_2}}} = K_{H_2} \quad \frac{N_{H_2O}}{p_{H_2O}} = \frac{K_{an}}{\sqrt{M_{H_2O}}} = K_{H_2O} \quad (4)$$

$$\frac{W_{an}}{P_{an}} = K_{an} \cdot (1-u) \cdot \sqrt{M_{H_2}} + u \cdot \sqrt{M_{H_2O}} \qquad (5)$$

where $K_{H2}$, $K_{H2O}$ are valve molar constant [kmol/(s atm)] for hydrogen and water, $N_{H2}$, $N_{H2O}$ [kmol/s] are molar flows and $P_{H2}$, $P_{H2O}$ are partial pressures [atm]. If $u > 70\%$, error of (5) is less than 7% compared to (3).

With the aim to obtain the partial pressure of hydrogen, the derivate of the perfect gas equation is applied, using the volume of the anode ($V_{an}$):

$$\frac{d}{dt}p_{H_2} = \frac{d}{dt}n_{H_2} \cdot \frac{R \cdot T}{V_{an}} = N_{H_2} \cdot \frac{R \cdot T}{V_{an}} \qquad (6)$$

The hydrogen molar flow ($q_{H2}$) has three relevant contributions: the input flow $N_{H2}^{in}$ the output flow $N_{H2}^{out}$ and the hydrogen flow that reacts $N_{H2}^{r}$.

$$\frac{d}{dt}p_{H_2} = \left(N_{H_2}^{in} - N_{H_2}^{out} - N_{H_2}^{r}\right) \cdot \frac{R \cdot T}{V_{an}} \qquad (7)$$

The hydrogen flow that reacts can be computed according to (8).

$$N_{H_2}^{r} = \frac{N_0 I}{2F} = 2K_r I \qquad (8)$$

where $F$ is the Faraday's constant [C/kmol], $N_0$ is the number of cells in series, $I$ is the stack current [A] and $K_r$ is model constant [kmol/(s A)] Therefore, (7) is rewritten as:

$$\frac{d}{dt}p_{H_2} = \left(N_{H_2}^{in} - N_{H_2}^{out} - 2K_r I\right) \cdot \frac{R \cdot T}{V_{an}} \qquad (9)$$

In conclusion, the hydrogen partial pressure is obtained by taking the Laplace transform while replacing the output flow from (4):

$$p_{H_2} = \frac{1/K_{H_2}}{1 + \tau_{H_2} S} \left(N_{H_2}^{in} - 2K_r I\right) \qquad (10)$$

where $\tau_{H2}$ is the time constant of the system pole associated with the hydrogen flow. Similar operations lead to obtaining partial pressure of other reactants and products.

According to Nernst's equation and Ohm's law (parameter $r$ represents ohmic losses), the stack voltage is computed as:

$$V = N_0 \left(E_0 + \frac{RT}{2F}\left[\ln\frac{p_{H_2}p_{O_2}^{0.5}}{p_{H_2O}}\right]\right) - r.Iv \qquad (11)$$

where $E_0$ [V] is the voltage associated with reaction free energy. Fig. 1 summarizes above equations and represents the SOFC model implemented in Simulink.
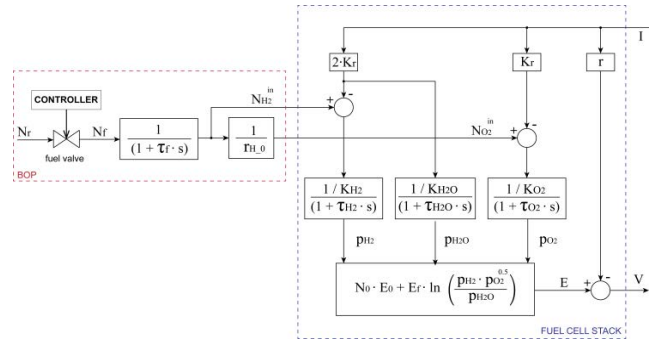


**FIGURE 1.** SOFC - block diagram.

## B. FUEL CELL LOCAL CONTROLLER

The fuel utilization factor is one of the most important parameters which affects the FC performances is [30]. The fuel utilization factor *u* is defined as the ratio between the rate of hydrogen that reacts and the rate of input hydrogen:

$$u = \frac{N_{H_2}^{in} - N_{H_2}^{out}}{N_{H_2}^{in}} = \frac{2K_r I}{N_{H_2}^{in}} \qquad (12)$$

The fuel utilization factor must be kept within a certain range. Indeed, overused-fuel conditions could result in permanent damage to the cells. On the other hand, underused-fuel conditions will rapidly lead to overvoltages. Furthermore, if the stack voltage output drops below a certain value, the power converter will not be able to manage the operating condition, it will lose synchronism and the SOFC will disconnect.

The power conditioner controls the output current for matching the required output power while maintaining the fuel cell within operational limits described above. When a change in the reference power occurs, the output current is changed as fast as possible for providing the required amount of power within a short time.

However, for maintaining a proper value of fuel utilization factor, current dynamic should be limited with regard to the dynamic of the fuel processor: Once maximum and minimum values for fuel utilization factor are set (0.9 and 0.7 in the model), current thresholds follow the dynamic of the input hydrogen flow:

$$i_{max}(t) = \frac{N_{H_2}^{in}(t) \cdot u_{max}}{2 \cdot K_r}, \quad i_{min}(t) = \frac{N_{H_2}^{in}(t) \cdot u_{min}}{2 \cdot K_r} \qquad (13)$$

The ideal current that allows the FC to provide the required power change continuously during a transient because voltage changes according to (11).

$$I_{ideal}(t) = \frac{P_{ref}}{V(t)}$$

$$= \frac{P_{ref}}{N_0 \left(E_0 + \frac{RT}{2F}\left[\ln\frac{p_{H_2}p_{O_2}^{0.5}}{p_{H_2O}}\right]\right) - r.I(t)} \qquad (14)$$

The output current is set by imposing limits defined in (13) to the ideal current, and the valve is controlled in order to obtain, in steady-state, the nominal fuel utilization factor.

The nominal utilization factor in steady state conditions is set to $u=0.8$ to ensure margins with respect to limits of 0.7 and 0.9 representing the safe operating area [29]. Thus, given a certain output current, the input hydrogen is as formulated in (15):

$$N_{H_2}^{in} = \frac{2K_r I}{0.8} \qquad (15)$$

In the model, power converter and its controller are considered as ideal components and their dynamics are neglected. Therefore, the Simulink implementation of chemical processes and control strategy discussed above imposes power values directly to a controllable load. Fig. 2 is a schematic representation of the SOFC system.
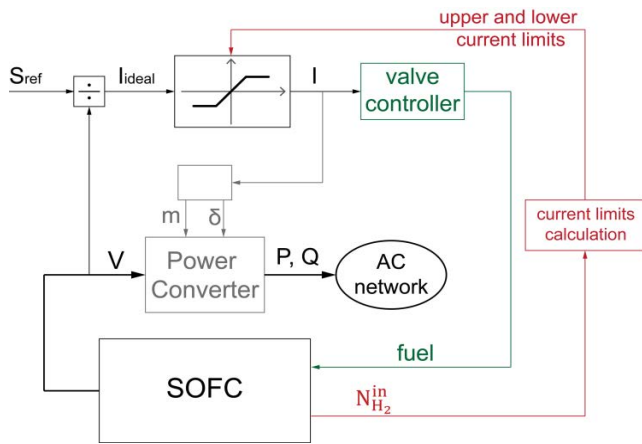


**FIGURE 2. SOFC system control and interface with the network.**

All the parameters used for FC modelling are based on a 100kW fuel cell model proposed in [30] and further enhanced with fuel processor model in [29]. The SOFC model is connected to low voltage lever in this work. However, the model can be connected to the medium voltage network, and its output power can be scaled up, with the aim of representing the aggregated behavior of several SOFC.

The dynamics of SOFC system response for the case of step change of power reference is illustrated in Fig. 3. Immediately after the reference changes, output power follows the reference thanks to the fast electrical response within fuel cells.
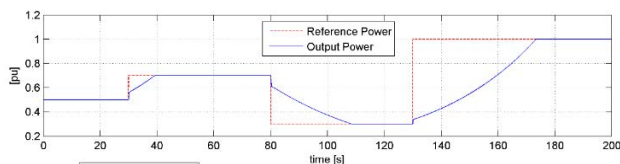


**FIGURE 3. SOFC system response.**

Although this fast response results in a relatively small change of output power, it is very beneficial for frequency support. The total response of SOFC system is slower due to dynamics of chemical process in fuel reformer. It ranges

from *10s* for the change in output power of *0.2 p.u.* to *30s* for the change of *0.4 p.u.* This dynamic can be sufficient for utilization of SOFC systems in primary frequency control.

The time response of SOFC system could be significantly reduced if a hydrogen storage is utilized and thus the slow dynamics of fuel reformer can be avoided.

### C. FREQUENCY DROOP CONTROL

In order to allow fuel cell systems participating in primary frequency regulation, a frequency controller must be implemented in the model.

The frequency controller for the FC power plants is designed following the Italian guidelines as an example for the demonstration purpose, and it is illustrated in Fig. 4. According to the Italian rules for frequency control by means of power plants which participate in the primary control, the power change in case of frequency variations ($\Delta f$) is determined as following:

$$\Delta P = -\frac{\Delta f}{f_0} \cdot \frac{P_n}{\sigma} \qquad (16)$$

The Italian TSO (TERNA) suggests a droop constant $\sigma$ in the range of *2-8%* for traditional generators. Furthermore, the frequency controller can have a dead zone of up to $\pm 10mHz$.
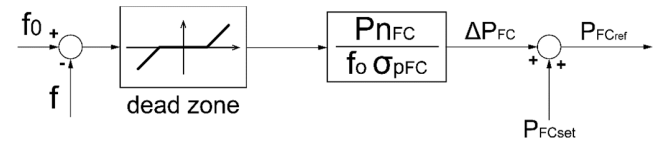


**FIGURE 4. Fuel cells' frequency controller.**

### D. PERFORMANCE INDICES

The traditional metric for examining the primary frequency control of a power system considers the steady-state frequency value after the action of primary controller. Although this method has been widely used, it does not provide an evaluation about the minimum frequency value reached during the transient.

Initially the detection of the lowest frequency point was not possible due to lack of appropriate tools, but, nowadays, it is possible and even necessary for the complete analysis of the frequency response. Indeed, the lowest value determines the action of load-shedding strategies or the disconnection of generators because of their under-frequency protection systems.

Since slope of the initial variation in frequency after a power imbalance depends on the systems' inertia, the minimum frequency value is determined by the combination of inertial response and primary regulation. Therefore, using a metric which considers the lowest value can be a good method to evaluate also the inertial behavior of the system.

Following the above-discussed considerations, in our case study, the metrics of frequency response introduced in [22]

are used for assessing the integration of renewable generation in the power system.

$$FRI_1 = \frac{Power\ unbalance[MW]}{f_{init} - f_{fin}} \quad (17)$$

$$FRI_2 = \frac{Power\ unbalance[MW]}{f_{init} - f_{min}} \quad (18)$$

where $f_{init}$, $f_{min}$ and $f_{fin}$ are respectively the frequency values before a disturbance occurs, the minimum value and the stabilized frequency after the action of primary frequency controllers.

The first metric ($FRI_1$) provides the leading information for assessing the adequacy of primary frequency control reserves.

Frequency response index 2 ($FRI_2$) is an evaluation of the inertial response and of the rate at which the power, which is used for restoring the generation-load balance. Indices 1 and 2 ((17) and (18)) are used for comparing system frequency performances with and without participation of FCs in two different scenarios.

In this work, the focus is on the initial 15-20 seconds after the power imbalance. This is the most critical period from the primary control perspective, because during this time, the frequency decline must be stopped to avoid reaching the set point of under-frequency load shedding scheme.

## III. TRANSMISSION-DISTRIBUTION GRID CO-SIMULATION

The simulations of TN and DN in a separate way and independently is no longer enough to catch all interactions of the two voltage level systems [33].

If the total inertia in the system is too low, a temporary power imbalance could cause deteriorated initial frequencies. Initially, the renewable generation units did not have any role in primary frequency control, because of the source uncertainty and the intention to exploit the renewable sources without margins.

Studies have been done to allow certain type of distributed generation (wind turbines, micro turbines and fuel cell) to contribute in primary frequency regulation [16].

Combined simulations of transmission and distribution networks are made by decoupling the model at the interconnection point. In our work, we dedicated two different digital real-time simulators for co-simulations:

–Distribution network model has been implemented in Simulink using Artemis solver from OPAL-RT and simulated using an OP5600 machine of OPAL-RT.

–Transmission network model has been developed in RSCAD and simulated on an RTDS simulator.

For local co-simulations, communication between real-time simulators is obtained thanks to an optic fiber connection between GPC card of the RTDS system and a Xilinx ML605 FPGA board, which is connected to OPAL-RT via PCIexpress as shown in Fig. 5.

In this setup, the RTDS simulator acts as a synchronization master by providing an external synchronization of the simulation time-step through the fiber optic link to the OPAL-RT
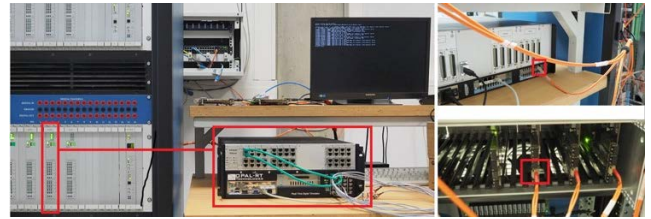


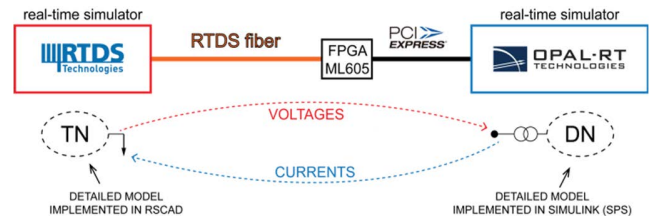**FIGURE 5.** Co-simulation setup showing the fiber interface.



**FIGURE 6.** Co-simulation setup.

system. Without this synchronization, a simultaneous start of the simulation and a concurrent execution of the simulation steps is not possible and causes a drift in time between the two subsystems which might result in a significant degradation of accuracy.

This digital connection allows exchanging voltage and current values between transmission and distribution network models (Fig. 6). Substantially, the interface used is an ideal transformer [34]:

–TN voltages are used as input values for controllable voltage sources that supply DN.

–DN currents are used as input values for controllable current sources, which represent the DN consumption, in the TN model.

It is important to evaluate fidelity of the interface between the two simulators, in order to ensure that the co-simulation is working properly and simulation results are reliable. For this purpose, time-step counters are sent and looped back by both simulators. Subtracting the current time-step counters from the loopback value yields the round-trip time (RTT) in multiples of the time-step period.

Long running tests have proven that the interface is capable of exchanging signals between simulators within a constant RTT of two time-steps (100 $\mu$s) without showing overruns. Albeit not applied in this study, such latencies are in a range which allow for compensation through Bergeron transmission lines by hiding the communication latency in the time-shift caused by travelling wave properties of the line.

Additionally, voltages and currents at the interface are monitored during the simulation from the RSCAD runtime console. As can be seen in Fig. 7, voltages and currents at the interconnection point are very similar in both simulators. Values showed here are collected during a voltage transient and, even in this situation, the interface guarantees reliability by communicating the right values.
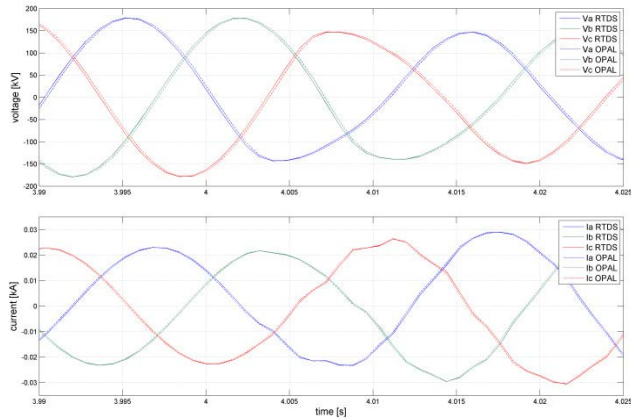
**FIGURE 7.** Voltages and currents at the interconnection point.

It should be noted that voltage waveforms have a monitoring delay that is the two times larger than currents' delay; since this data is collected from RTDS. Namely, voltage waveforms from OPAL are plotted after being sent to the RSCAD runtime console through the interface, thus doubling the delay time. Therefore, voltages from OPAL here plotted have one time step delay because of the communication from RTDS to OPAL and another time-step delay due to the communication between OPAL and the runtime console in the RSCAD software.

## IV. CENTRALIZED CONTROL STRATEGY

The frequency control strategy for FC systems described in Section II is applied to each FC system installed in the DN represented with detailed models, and it is thus used as a local controller. Besides the local controller, by which each fuel cell autonomously varies its output power, a centralized controller for FCs is implemented. This controller mainly aims to support frequency regulation by coordinating FCs in DNs, however it is also possible to improve the voltage profile along distribution feeders by controlling the reactive power provided by FCs at certain buses.

This voltage profile improvement during incidences or frequency disturbances leads to maintain the required voltage for DGs with voltage ride-through capability to remain connected. Therefore, further power imbalance and frequency deviation in the system can be avoided. The centralized controller is based on a simple logic with the main goal to demonstrate how different control objectives or strategies reflect to system performances in providing frequency support. We demonstrate that controlling the output reactive power to improve voltage profile as instance could indirectly improve system frequency.

The centralized controller considers that a SOFC plant is not an infinite source (or sink) of reactive power, the maximum reactive power that it can provide at each instant is determined by its fixed apparent power capability and the instantaneous real power generation:

$$|Q| \le \sqrt{S^2 - P^2} \qquad (19)$$

Obviously, the active power output can be reduced if the most important objective is voltage support. Our implemented controller considers the scheduled $P$ and $Q$ output ($P_{set}$, $Q_{set}$) of each fuel cell system and uses the residual margin for frequency and voltage support ($\Delta P$, $\Delta Q$).

$$\sqrt{(P_{set} + \Delta P)^2 + (Q_{set} + \Delta Q)^2} \le S_{max} \qquad (20)$$

When additional active and reactive powers are required at the same time, the controller utilizes the inverter capability in different ways by giving priority to frequency or voltage support.

If the priority of the controller is given to ''frequency'', the required $\Delta P$ will be provided and the residual capability margin will be used for reactive power. Vice versa, if the voltage support has the priority, the reactive power will be guaranteed (without exceeding the inverter capability limit) and active power for frequency control will be provided only if possible according to the inverter capability characteristic.

Each FC system sends the voltage measurements at its bus to the controller and receives $\Delta P$ and $\Delta Q$ values computed according to the control strategy. Fig. 8 gives an overview of the control algorithm which determines the references $\Delta P$ and $\Delta Q$ for each SOFC system following the selected control strategy and calculated $\Delta P_r$ and $\Delta Q_i$ based on droop characteristics.

In Fig. 9 a schematic illustration of the centralized controller and its communications with fuel cell systems is presented. Control strategies and the diagram are explained in the following section where different test cases of this study are introduced.

Considering both local and centralized controllers, four control strategies are designed and compared for managing FC systems in the DNs. Each control strategy has been tested with two different penetration levels of fuel cell systems in a detailed DN model, while additional simulations provide the frequency behavior when FC systems do not participate in frequency regulation.

To get clear solution of the problem supported by thorough and internal investigations in the under study DN we use detailed model of a DN. Other DNs can be represented by equivalent models, which reproduce the behavior of the real network as realistic as possible without demanding too much computational power.

We developed an equivalent and modular model for DN. Modularity means that parts of the model can be easily added or removed according to the necessities, thereby maintaining the model as less demanding as possible in terms of computational power.

The following subsections describe control strategies applied to fuel cells installed in the detailed distribution network. When enabled, grid support of fuel cells in equivalent DNs is limited to frequency control. Furthermore, the droop constant has been always set to 2% for every fuel cell system.
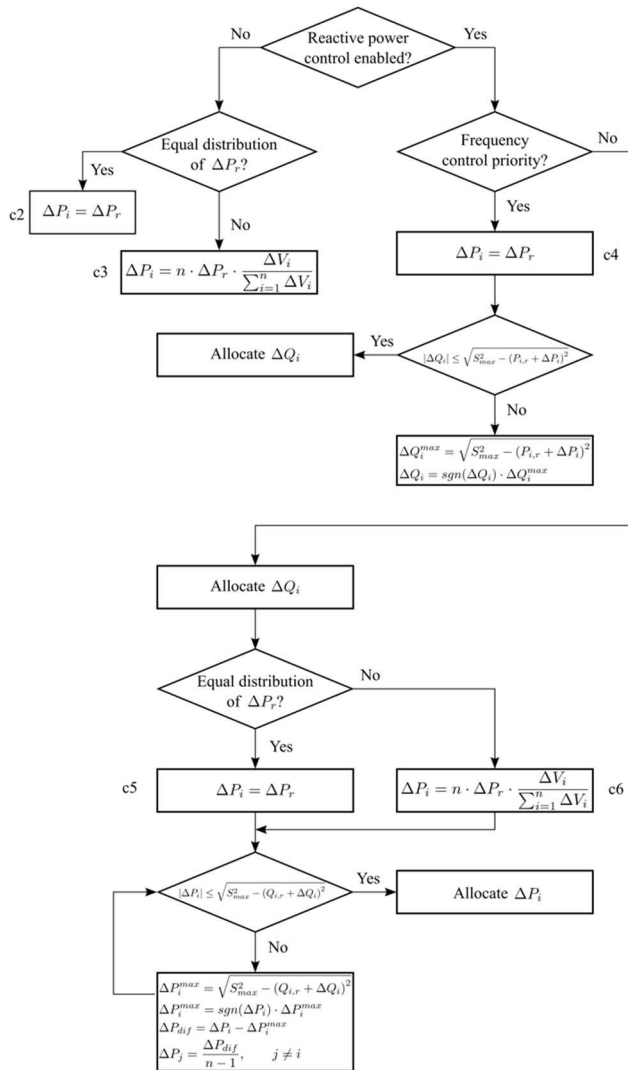
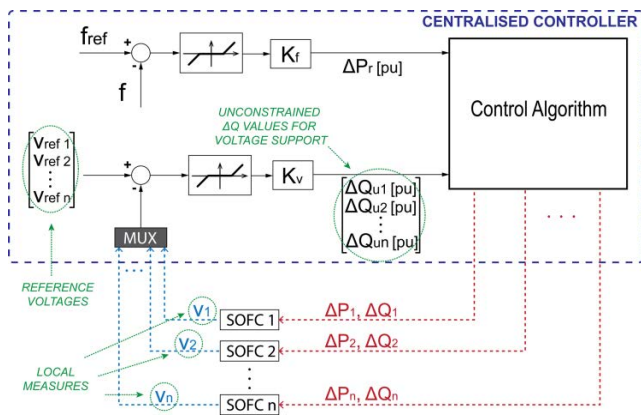**FIGURE 8.** Flowchart of centralized control algorithm.



**FIGURE 9.** Centralized controller for fuel cells.

## A. TEST CASE "C0": REFERENCE SYSTEM RESPONSE

In this scenario the fuel cells do not participate in frequency regulation. This simulation provides the frequency behavior of the system when only conventional power plants compensate frequency deviations. This test case is used as a reference for evaluating the effectiveness of FC participation in primary frequency control.

## B. TEST CASE "C2": ACTIVE POWER CONTROL WITH EQUAL PARTICIPATION OF SOFC UNITS

The centralized controller computes the additional active power required for frequency support and equally share (in per-unit) this amount among fuel cells installed in the DN. The voltage support is disabled in this case; therefore, no additional reactive power is provided by fuel cells in case of low-voltage observation. The objective of this test case is to demonstrate the performance of the simplest approach to frequency support without considering voltage profiles.

## C. TEST CASE "C3": ACTIVE POWER CONTROL WITH VOLTAGE-DEPENDENT PARTICIPATION OF SOFC UNITS

In simulation "c3", the voltage support with reactive power is not enabled in centralized controller, the same as in simulation "c2". However, the total active power required for frequency support is partitioned among fuel cells considering the local voltage levels. Where the voltage level is more critical, a larger amount of active power is generated. This method aims to provide local active power generation where needed to reduce the total power flow along a feeder which compensates voltage drop and improves its voltage profile. The objective is to determine whether this method could improve voltage profile without including reactive power control.

## D. TEST CASE "C4" – ACTIVE AND REACTIVE POWER CONTROL WITH FREQUENCY CONTROL PRIORITY

Both active and reactive power control are enabled in centralized control. Frequency control priority is considered, thus in first step the centralized controller computes the active power required for frequency support based on droop characteristic and equally divides (in per-unit) this amount among fuel cells installed in the DN. The remaining inverter capability is then used for providing reactive power for voltage support. Since the voltage can vary substantially along distribution feeders, the reactive power that would be necessary for voltage support is different for every fuel cell. The objective of this test case is to compare the cases of frequency control priority and voltage control priority. Voltage control priority is analyzed in the test cases below.

## E. TEST CASE "C5" VOLTAGE CONTROL PRIORITY WITH EQUAL ACTIVE POWER PARTICIPATION OF SOFC UNITS

In this strategy, the main purpose is to improve voltage profile. Firstly, the required additional reactive power is allocated for each FC system. The controller, then, tries to equally share the additional active power request for frequency control among all fuel cells. Since the frequency is a global variable inside DN, when a FC system is not able to provide its portion of active power, because of the inverter capability limitations,

that power is provided by other fuel cells. This algorithm, which redistributes the missing active power, is repeated until all the required $\Delta P$ is allocated, or until the capability limit of every inverter is reached. In this way, the maximum possible amount of the required active power is provided.

### F. TEST CASE "C6": VOLTAGE CONTROL PRIORITY WITH VOLTAGE-DEPENDENT ACTIVE POWER PARTICIPATION OF SOFC UNITS

Similar to strategy of test case "C4", the controller dispatches firstly the reactive power and then uses the remaining capability for frequency control. However, here in "c6", the active power is divided among fuel cells considering also the voltage levels. Where the voltage level is more critical, a larger amount of active power is generated. This aims to improve voltage profile by reducing voltage drop along certain parts of the feeders. When the maximum capability of one inverter is reached, the missing active power is redistributed among other FCs like in simulation case "C5".

The control strategies in c2 to c6 have been tested also with the higher FCs' penetration level ("c2_h" to "c6_h").

## V. CASE STUDY AND SIMULATION RESULTS

Simulations are carried out in a real-time mode thanks to the developed platform of interconnected real-time simulators: the OPAL-RT real-time simulator is connected to an RTDS rack through a GTFPGA card. European configuration of transmission and distribution network models proposed by CIGRé [31] for studying DERs integration, are implemented. The medium voltage network is modelled in MATLAB/ Simulink for real-time simulation on OPAL-RT using a fixed-step solver for power systems (ARTEMiS) provided by OPAL-RT. The high-voltage transmission benchmark model is implemented in RSCAD, which is the dedicated software of RTDS real-time simulator.

According to the considerations above, PV and SOFC systems are modelled, considering their features from the network perspective. PV model includes LVRT capability required for distributed generation according to the Italian grid code.

In scope of the analysis of transmission-distribution system interactions, different scenarios of frequency control by FC systems are considered [32]. FC systems are used to support the primary frequency response of the electrical power system. Different control strategies for using the capability of inverters that connect SOFCs to the network are tested, and the voltage support through reactive power injection is included in the investigation.

### A. CASE STUDY

The European configuration of the TN benchmark (Fig. 10), is a three-phase high voltage network with ideal transposition and solidly grounded ground wires. Four large synchronous generators provide power to constant-impedance loads through the 13-bus network.
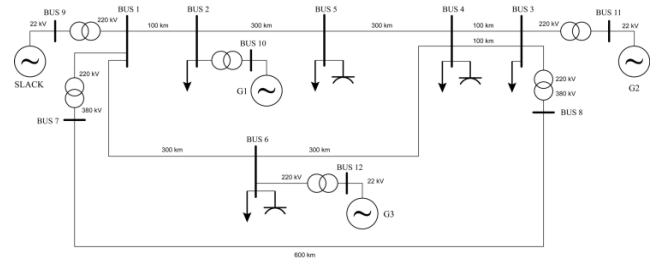


**FIGURE 10.** Topology of european high voltage TN benchmark.
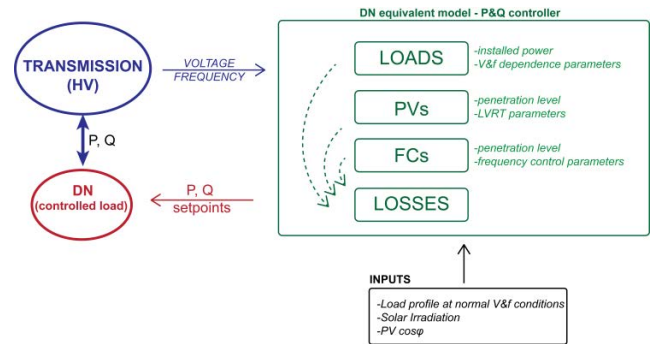


**FIGURE 11.** Equivalent model for DNs - conceptual scheme.

The rated line-to-line voltages are 220 kV and 380 kV, and nominal frequency is 50 Hz. Furthermore, three fixed capacitor banks support the voltage by injecting reactive power in the network. Physical models of synchronous generators with turbine governors and exciters represent generators.

Depending on the needs of the simulation, certain portions of the constant loads have been replaced by the detailed DN model simulated in OPAL-RT or by an appropriate equivalent DN model.

The developed DN equivalent model consists of a local controller that imposes active and reactive power values of a controllable load (Fig. 11). Voltage and frequency at the interconnection point are measured on the transmission network and are sent to the controller.

Other inputs, such as load profile and solar irradiation, allow for having more realistic behavior. The controller contains also parameters for calibrating the model depending on the network to be represented (installed load power, PV penetration, etc.). The controller consists of four modules: loads, PVs, FCs and losses.

The aggregated loads behavior incorporates load profiles and dependencies of voltage and frequency:

$$P_L(t) = P_{L0}(t) \cdot \left(\frac{V(t)}{V_0}\right)^{\alpha} \cdot \left(1 + K_{Pf} \cdot \frac{\Delta f}{f_0}\right) \quad (21)$$

$$Q_L(t) = Q_{L0}(t) \cdot \left(\frac{V(t)}{V_0}\right)^{\beta} \cdot \left(1 + K_{Qf} \cdot \frac{\Delta f}{f_0}\right) \quad (22)$$

Equations (21) and (22) have been therefore implemented in the model. $P_{L0}$ and $Q_{L0}$ inputs respectively represent active and reactive power profiles at nominal voltage and frequency

values. Parameters $K_{Pf}$, $K_{Qf}$, $\alpha$ and $\beta$ define the frequency and voltage dependence of loads.

The essential features of the PVs' behavior that have been considered to develop the controller are:

–Dependence on solar irradiation

–Voltage disconnection with LVRT capability

–Reconnection algorithm after low voltage tripping

The solar irradiation is the model input, while $cos\varphi$ of PV power generation and photovoltaic penetration level can be set as necessary. Disconnection and reconnection times as well as low voltage thresholds can be calibrated according to system operator rules.

The essential features of SOFC systems participating in frequency control that have been considered to develop the controller are:

–Feasible operating area of fuel cell stacks according to maximum and minimum values of fuel utilization factor;

–Dynamic behavior affected by chemical processes;

–Frequency controller that allows FC systems to participate in primary frequency regulation.

Since power absorption due to ohmic losses is proportional to the square of the current, a simply calculation is made inside the controller.

$$P_{\text{Loss}} \propto I^2 \Rightarrow P_{\text{Loss}}$$
$$= \left( \frac{\sqrt{(P_{\text{load}} - P_{DG})^2 + (Q_{\text{load}} - Q_{DG})^2}}{V} \right)^2 K_{\text{loss}} \tag{23}$$

The total current of the distribution network is considered for computing ohmic losses by using the parameter $K_{loss}$ as proportionality factor. $K_{loss}$ depends on the overall ohmic losses of the real DN and must be calibrated depending on the real network.

Part of the total reactive power absorbed by a distribution network is due to lines and transformers. For including such contribution in the equivalent model for DNs, the overall inductive and capacitive behavior of these components is approximated by implementing (24) and (25) in the controller.

$$Q_{ind} \propto I^2 \Rightarrow \tag{24}$$
$$Q_{ind} = \left( \frac{\sqrt{(P_{\text{load}} - P_{DG})^2 + (Q_{\text{load}} - Q_{DG})^2}}{V} \right)^2 K_{\text{ind}}$$
$$Q_{cap} \propto V^2 \Rightarrow Q_{cap} = V^2 \cdot K_{cap} \tag{25}$$

The contribution of lines and transformers to the reactive power absorbed is therefore implemented as the difference between the inductive contribution ($Q_{ind}$) and the capacitive contribution ($Q_{cap}$).

The European configuration of the DN benchmark is a three-phase medium voltage network with two transformers and two feeders and it is based on a real network in the southern Germany, which provides electric power to a small town and its surrounding rural area. The rated line-to-line voltage is 20 kV and nominal frequency is 50 Hz. Industrial
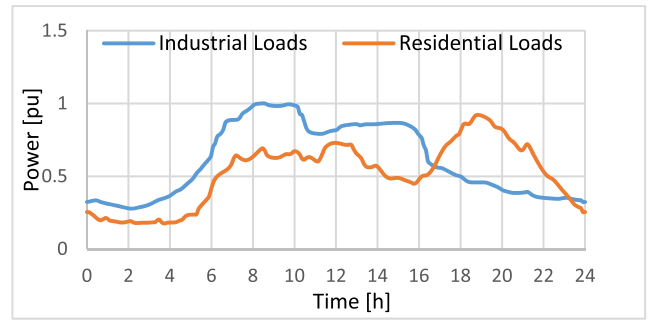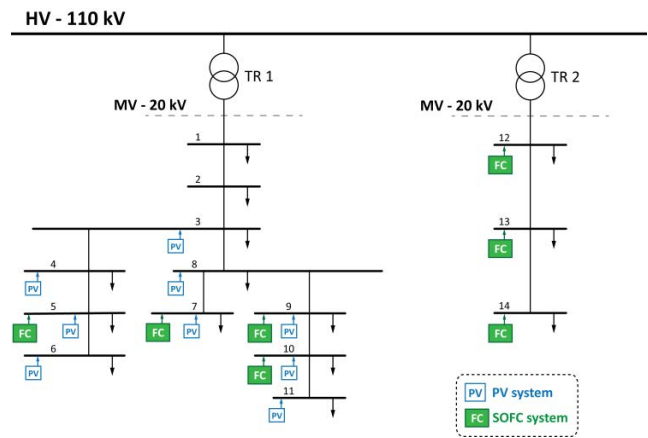


**FIGURE 12.** Load profiles.



**FIGURE 13.** SOFC systems placement in MV benchmark network.

and residential loads have a total installed power of 46,215 MVA and load values follow load profiles showed in Fig. 12. These profiles are proposed by CIGRé in [31] together with the benchmark networks.

For analyzing the system's frequency response, this medium-voltage benchmark network has been used as detailed model for one distribution network considering a photovoltaic penetration level of 6.9 %. Seven SOFC systems have been placed according to Fig. 13 in this DN for providing frequency support.

CIGRé's report suggests using an 110kV sub-transmission line for connecting this DN benchmark to the TN benchmark described above. Two identical 110 kV lines are therefore used for supplying the two transformers.

These lines are very useful for implementation in OPAL-RT because they allow dividing the model across different cores of the real-time simulator. In fact, sub-transmission lines can be designed for introducing a delay of one time step, which is required by OPAL-RT to execute the model on multiple cores. Splitting the model across different cores is necessary for the real time simulation. DN is not computationally intensive considering the number of nodes, but given the number of components that will be connected (PV and fuel cell systems), one single core does not have enough computational resources to avoid overruns.
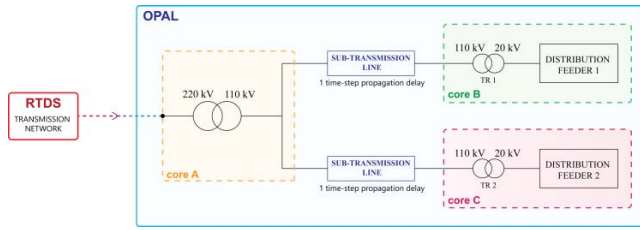
**FIGURE 14.** Split-up into OPAL cores.

Fig. 14 is a schematic representation of model partitioning among three OPAL-RT cores. The interface for OPAL-RTDS co-simulations and the 220/110 kV transformer are executed on one core, while each distribution feeder is implemented on a dedicated core.

### B. CASE SCENARIO

In this work, the fuel cell systems are considered as a resource available to system operators for supporting the network operation in case of critical circumstances. As discussed in [35], SOFC systems are capable to withstand larger voltage sags than specified by LVRT considered in this paper and illustrated in Fig. 15.
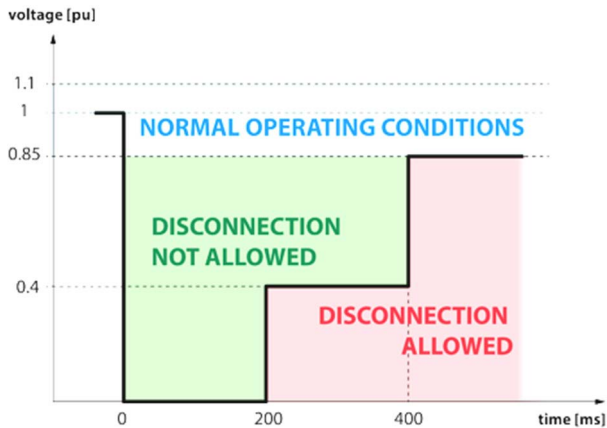


**FIGURE 15.** LVRT curve for DGs in italy.

Namely, SOFC system can maintain its normal operation even with voltage sags of *0.2 p.u.* which resulted in minimal transient effects on SOFC operation. As in our scenario voltage levels of SOFC buses do not drop below *0.8 p.u.* during analyzed transients, SOFC systems do not disconnect in case of low-voltage level, yet stay connected. This is not the case for PV systems that follow Italian regulation for LVRT requirements, illustrated in Fig. 15.

Two different FCs' penetration levels have been tested: a total installed power of 1.4 MW and a higher level, namely 3.5 MW of installed fuel cells' power. We analyze the effectiveness of FCs' participation in primary frequency regulation when a sudden change in weather conditions causes a power imbalance in scenarios with high level of PV penetration.
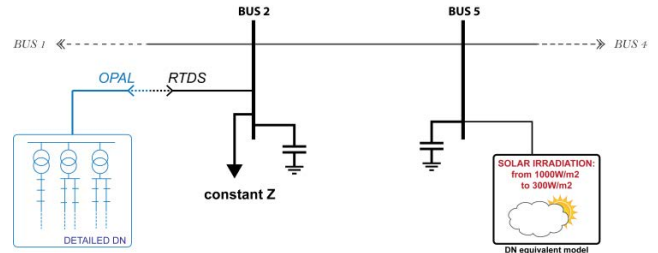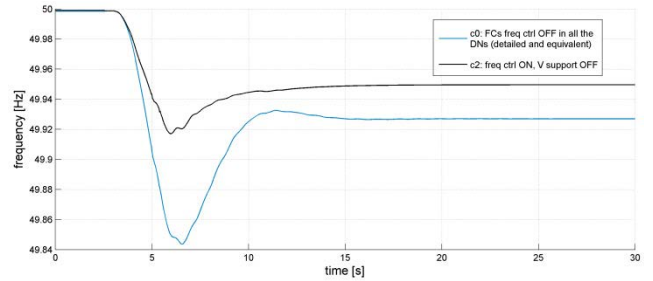


**FIGURE 16.** Scenario case.



**FIGURE 17.** Frequency at TN's bus 8 - without and with FC participation (test cases c0 and c2).

The generator G1 connected (according to CIGRé) to TN's bus number 2 was disconnected for representing the shut-off of traditional generators that are not dispatched because they were replaced by a large number of DGs. Here, the power imbalance between generation and load is caused by a reduction in solar irradiation in the area of the DN (equivalent model) connected to TN's bus 5 (Fig. 17).

Besides the equivalent model that represents this DN, loads of other three buses have been partly replaced by the equivalent model that emulates the participation of FCs in frequency support. Table 1 and Table 2 contain the data used for constant-impedance loads and equivalent DN model as well as the resulting aggregate properties for case scenario.

**TABLE 1.** Aggregate DNs' data.

| BUS | Aggregate DNs' Data | | | |
| | P (net value) [MW] | Q (net value) [MVAR] | Penetration of PV [%] | Penetration of FC [%] |
|---|---|---|---|---|
| 3 | 325.20 | 245.42 | 19.46 | 21.62 |
| 4 | 326.13 | 240.46 | 15.70 | 22.83 |
| 5 | 110.88 | 157.98 | 40.00 | 0.00 |
| 6 | 425.50 | 291.05 | 16.19 | 32.39 |

The reduction of PV generation in distribution network (equivalent model) connected to bus 5 is assumed as the generation loss as the cause for frequency decline. Therefore, it is used for computing frequency metrics.

Any other PV disconnection in other distribution network is considered as a result of an event in DN at TN's bus 5.

**TABLE 2.** Constant-Z loads and equivalent DN models.

| BUS | Constant-Z load | | | | | Equivalent DN model | | |
|---|---|---|---|---|---|---|---|---|
| | P [MW] | Q [MVAR] | Installed Load[MW] | Loads cosφ | Load profile [pu] | Penetration of PV [%] | PV cosφ | Installed FC [MW] |
| 3 | 162.5 | 122 | 300 | 0.9 | 1 | 30 | 0.97 | 100 |
| 4 | 163 | 122 | 275 | 0.88 | 1 | 25 | 0.9 | 100 |
| 5 | 0 | 0 | 495 | 0.91 | 0.6 | 40 | 0.94 | 0 |
| 6 | 217.5 | 148 | 400 | 0.91 | 1 | 25 | 0.92 | 200 |
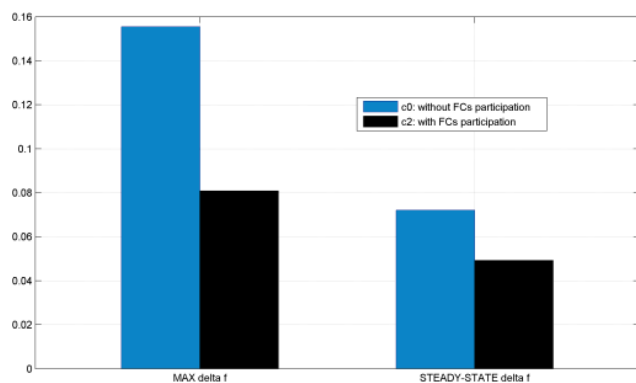


**FIGURE 18.** Comparison of maximum and steady-state Δf (test cases c0 and c2).



**FIGURE 19.** Voltage at buses 5, 7, 9 and 10 of the detailed DN.
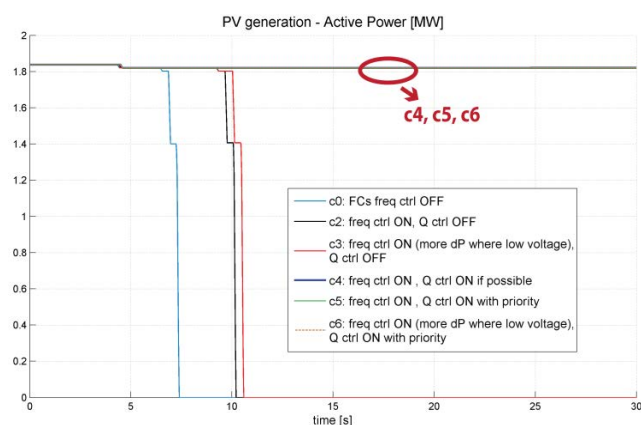


**FIGURE 20.** Active power generation from PVs installed in the equivalent DN.

This assumption is made with the aim to identify a common initial cause for all the simulations. Strategies that avoid PV's disconnection will hence result better, since they reduce the net power imbalance between generation and loads.

Since PVs in the DN at bus 5 disconnect after the drop in solar irradiation level, the Δ*P*, which causes the frequency decline, is the PV generation power in this distribution network before the perturbation: 184 MW.

### C. SIMULATION RESULTS
Fig. 17 illustrates the improvement in frequency response achieved thanks to the participation of SOFCs in primary frequency regulation. When fuel cells do not contribute to frequency regulation (simulation c0): during the transient, the frequency reaches the minimum value of 49.844 Hz and then it is stabilized at 49.927 Hz.

EG is computed as the ratio between the power imbalance (it is the reduction of PVs in the equivalent DN at bus 5: 184 MW) and the steady state frequency error, which is 0.0721Hz.

Fig. 18 compares both maximum and steady state Δ*f* in case without and with FC participation in frequency regulation (simulation c0 and c2).

The control strategy used for managing fuel cells strongly affects voltage profiles in the distribution feeders. The reactive power provided by SOFCs in simulations c4, c5 and c6
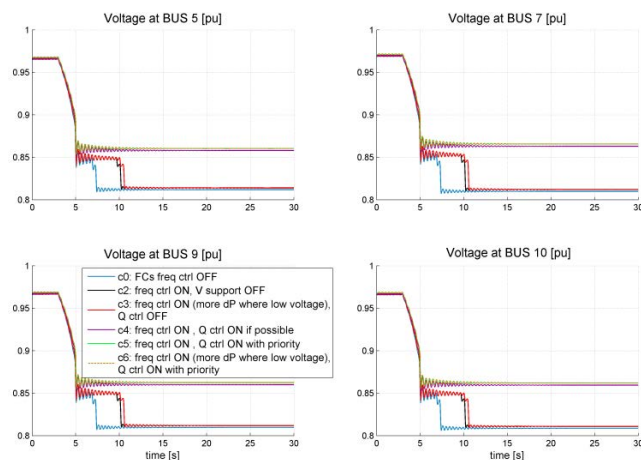
result in voltage levels along feeders which are higher than the disconnection threshold for PVs (we set *0.85 p.u.* just to examine Italian LVRT regulation shown in Fig. 15).

Therefore, photovoltaic systems remain connected to the detailed DN model in simulations c4, c5 and c6. Fig. 19 shows data about voltages along the feeder 1 of the detailed distribution network model.

Obviously, the detailed DN withdraws less active and reactive power when photovoltaic systems do not disconnect. The total PV generation within the detailed DN is illustrated in Fig. 20 for different control strategies.

It must be noted that the control strategy ''c3'' does not avoid the disconnection of PV generators; it allocates larger portions of active power to those buses where the voltage level is more critical but does not involve reactive power. Its only effect is to barely delay the disconnection compared to the strategy in which the additional active power for frequency support is equally divided among SOFC systems (c2).

In terms of steady state frequency value following the primary regulation, strategies that allow PVs to stay connected by providing reactive power for voltage support prove

**TABLE 3.** Simulations' results - frequency metrics.

| Simulation | f0 [Hz] | f∞ [Hz] | fmin [Hz] | FRI1 [MW/Hz] | FRI2 [MW/Hz] |
|---|---|---|---|---|---|
| c0 | 49.9991 | 49.9270 | 49.8436 | 2552.7 | 1183.4 |
| c2 | 49.9988 | 49.8596 | 49.9180 | 3741.4 | 2278.1 |
| c3 | 49.9988 | 49.9495 | 49.9180 | 3734 | 2276.8 |
| c4 | 49.9988 | 49.9501 | 49.9175 | 3782.8 | 2263.7 |
| c5 | 49.9988 | 49.9501 | 49.9174 | 3782.6 | 2260.7 |
| c6 | 49.9988 | 49.9501 | 49.9175 | 3783.6 | 2263.9 |

**TABLE 4.** Simulations' results - frequency metrics (higher FC penetration level).

| Sim. | f0 [Hz] | f∞ [Hz] | fmin [Hz] | FRI1 [MW/Hz] | FRI2 [MW/Hz] |
|---|---|---|---|---|---|
| c2_h | 49.9997 | 49.9512 | 49.9186 | 3789.9 | 2266.9 |
| c3_h | 49.9997 | 49.9512 | 49.9190 | 3791.8 | 2279.5 |
| c4_h | 49.9998 | 49.9504 | 49.9173 | 3727.2 | 2230.2 |
| c5_h | 49.9996 | 49.9504 | 49.9177 | 3737.7 | 2244.8 |
| c6_h | 49.9997 | 49.9504 | 49.9174 | 3728.9 | 2234.4 |

to be more effective, even though the participation of FCs' in frequency regulation is completely annulled. Actually, these strategies indirectly involve FCs in frequency support. Although improvement of voltage levels in the transmission network results in an increase of consumption of constant-Z loads, but this effect is negligible compared to the power provided by PV systems installed in the detailed network. Therefore, strategies c5 and c6 ensure better performance compare to strategies that do not consider the voltage support through injection of reactive power at specified DN's nodes.

## VI. CONCLUSION

High penetration of DGs in DNs brings new challenges for power system stability control. One of the challenges are due to creation of low inertia systems. However, applying appropriate control strategies could exploit some of DGs in DNs to provide frequency and voltage support for the whole system. We presented a developed centralized coordinated scheme to control SOFC systems aiming at mitigation of system frequency deviation.

Different scenarios are created to demonstrate different configurations of the control scheme in prioritizing voltage and frequency regulation. Although the main objective of the control scheme in all cases is to support primary frequency regulation, but there are scenarios in which the scheme chooses to firstly regulate voltage to make frequency

deviation corrected. The simulation results prove that the use of SOFC systems for primary frequency regulation are a promising solution if an appropriate control strategy is in place. Due to the fast response of SOFCs, the inertial frequency response is improved significantly as well as primary regulation.

Furthermore, since fuel cell systems are easily controllable and do not rely on an intermittent energy resource, their participation in frequency control is guaranteed regardless to weather conditions. Under certain conditions, exploiting the FCs inverter capability for providing voltage support through reactive power injections instead of for providing active power can be more effective even from a frequency response point of view. In summary, if the voltage improvement avoids the disconnection of distributed generation, the resulting effect is a lower power imbalance and, consequently a better frequency response.

## REFERENCES

[1] S. O. Muhanji, A. Muzhikyan, and A. M. Farid, "Distributed control for distributed energy resources: Long-term challenges and lessons learned," *IEEE Access*, vol. 6, pp. 32737–32753, 2018, doi: 10.1109/ACCESS.2018.2843720.

[2] T. Kerdphol, F. S. Rahman, Y. Mitani, M. Watanabe, and S. Küfeoğlu, "Robust virtual inertia control of an islanded microgrid considering high penetration of renewable energy," *IEEE Access*, vol. 6, pp. 625–636, 2018, doi: 10.1109/ACCESS.2017.2773486.

[3] R. Li, W. Wang, and M. Xia, "Cooperative planning of active distribution system with renewable energy sources and energy storage systems," *IEEE Access*, vol. 6, pp. 5916–5926, 2018, doi: 10.1109/ACCESS.2017.2785263.

[4] A. Cagnano, E. De Tuglie, M. Liserre, and R. A. Mastromauro, "Online optimal reactive power control strategy of PV inverters," *IEEE Trans. Ind. Electron. Control Instrum.*, vol. 58, no. 10, pp. 4549–4558, Oct. 2011.

[5] M. Stevic, A. Estebsari, S. Vogel, E. Pons, E. Bompard, M. Masera, and A. Monti, "Multi-site European framework for real-time co-simulation of power systems," *IET Gener. Transmiss. Distrib.*, vol. 11, no. 17, pp. 4126–4135, Nov. 2017.

[6] M. E. Hernandez, G. A. Ramos, M. Lwin, P. Siratarnsophon, and S. Santoso, "Embedded real-time simulation platform for power distribution systems," *IEEE Access*, vol. 6, pp. 6243–6256, 2018, doi: 10.1109/ACCESS.2017.2784318.

[7] A. Estebsari, E. Pons, T. Huang, and E. Bompard, "Techno-economic impacts of automatic undervoltage load shedding under emergency," *Electr. Power Syst. Res.*, vol. 131, pp. 168–177, Feb. 2016.

[8] W. Ju, K. Sun, and R. Yao, "Simulation of cascading outages using a power-flow model considering frequency," *IEEE Access*, vol. 6, pp. 37784–37795, 2018, doi: 10.1109/ACCESS.2018.2851022.

[9] E. Bompard, A. Monti, A. Tenconi, A. Estebsari, T. Huang, E. Pons, M. Stevic, S. Vaschetto, and S. Vogel, "A multi-site real-time co-simulation platform for the testing of control strategies of distributed storage and V2G in distribution networks," in *Proc. 18th Eur. Conf. Power Electron. Appl. (EPE ECCE Europe)*, Karlsruhe, Germany, 2016, pp. 1–9, doi: 10.1109/EPE.2016.7695666.

[10] B. Palmintier, E. Hale, T. M. Hansen, W. Jones, D. Biagioni, H. Sorensen, H. Wu, and B.-M. Hodge, "IGMS: An integrated ISO-to-appliance scale grid modeling system," *IEEE Trans. Smart Grid*, vol. 8, no. 3, pp. 1525–1534, May 2017.

[11] J. C. Boemer, B. G. Rawn, M. Gibescu, M. A. M. M. Meijden, and W. L. Kling, "Response of wind power park modules in distribution systems to transmission network faults during reverse power flows," *IET Renew. Power Gener.*, vol. 9, no. 8, pp. 1033–1042, Nov. 2015.

[12] B. Palmintier, E. Hale, T. Hansen, W. Jones, D. Biagioni, K. Baker, H. Wu, J. Giraldez, H. Sorensen, M. Lunacek, N. Merket, J. Jorgenson, and B.-M. Hodge, "Final technical report: Integrated distribution-transmission analysis for very high penetration solar PV," Nat. Renew. Energy Lab., Golden, CO, USA, Tech. Rep. NREL/TP-5D00-65550, 2016.

[13] *Smart Net*. Accessed: Feb. 12, 2019. [Online]. Available: http://smartnet-project.eu/

[14] M. Benini, S. Canevese, D. Cirio, and A. Gatti, "Battery energy storage systems for the provision of primary and secondary frequency regulation in Italy," in *Proc. IEEE 16th Int. Conf. Environ. Electr. Eng. (EEEIC)*, Florence, Italy, Jun. 2016, pp. 1–6.

[15] M. Swierczynski, D. I. Stroe, A. I. Stan, and R. Teodorescu, "Primary frequency regulation with Li-ion battery energy storage system: A case study for Denmark," in *Proc. IEEE ECCE Asia Downunder*, Melbourne, VIC, Australia, Jun. 2013, pp. 487–492.

[16] J. Morren, S. W. D. Haan, and J. Ferreira, "Primary power/frequency control with wind turbines and fuel cells," in *Proc. IEEE Power Eng. Soc. Gen. Meeting*, Jun. 2006, pp. 1–8.

[17] P. C. Sekhar and S. Mishra, "Storage free smart energy management for frequency control in a diesel-PV-fuel cell-based hybrid AC microgrid," *IEEE Trans. Neural Netw. Learn. Syst.*, vol. 27, no. 8, pp. 1657–1671, Aug. 2016.

[18] K. V. Vidyanandan and N. Senroy, "Frequency regulation in a wind–diesel powered microgrid using flywheels and fuel cells," *IET Gener., Transmiss. Distrib.*, vol. 10, no. 3, pp. 780–788, Feb. 2016.

[19] S. Kayalvizhi and D. M. V. Kumar, "Load frequency control of an isolated micro grid using fuzzy adaptive model predictive control," *IEEE Access*, vol. 5, pp. 16241–16251, 2017.

[20] K. R. Sree and A. K. Rathore, "Impulse commutated high-frequency soft-switching modular current-fed three-phase DC/DC converter for fuel cell applications," *IEEE Trans. Ind. Electron.*, vol. 64, no. 8, pp. 6618–6627, Aug. 2017.

[21] X. Liu and H. Li, "An electrolytic-capacitor-free single-phase high-power fuel cell converter with direct double-frequency ripple current control," *IEEE Trans. Ind. Appl.*, vol. 51, no. 1, pp. 297–308, Jan./Feb. 2015.

[22] J. H. Eto, "Use of frequency response metrics to assess the planning and operating requirements for reliable integration of variable renewable generation," Lawrence Berkeley Nat. Lab., Berkeley, CA, USA, Tech. Rep., 2011.

[23] Y. Xu, C. Li, Z. Wang, N. Zhang, and B. Peng, "Load frequency control of a novel renewable energy integrated micro-grid containing pumped hydropower energy storage," *IEEE Access*, vol. 6, pp. 29067–29077, 2018, doi: 10.1109/ACCESS.2018.2826015.

[24] M. Elsisi, M. Soliman, M. A. S. Aboelela, and W. Mansour, "Model predictive control of plug-in hybrid electric vehicles for frequency regulation in a smart grid," *IET Gener., Transmiss. Distrib.*, vol. 11, no. 16, pp. 3974–3983, 2017.

[25] M. H. Nehrir and C. Wang, *Modeling and Control of Fuel Cells*. Piscataway, NJ, USA: IEEE Press, 2009.

[26] F. Gao, M. Kabalo, B. Blunier, and A. Miraoui, "Fuel cell systems," in *Power Electronics for Renewable and Distributed Energy Systems* (Green Energy and Technology). Golden, CO, USA: Springer, 2013, pp. 185–234.

[27] S. Chowdhury, S. Chowdhury, and P. Crossley, "Appendix D: Application of solid-oxide fuel cell in distributed power generation," in *Proc. Int. Conf. Microgrids Act. Distrib. Netw.*, London, U.K., 2009, pp. 215–226.

[28] Y. Zhu and K. Tomsovic, "Development of models for analyzing the load-following performance of microturbines and fuel cells," *J. Electr. Power Syst. Res.*, vol. 62, no. 1, pp. 1–11, May 2000.

[29] Y. H. Li, S. S. Choi, and S. Rajakaruna, "An analysis of the control and operation of a solid oxide fuel-cell power plant in an isolated system," *IEEE Trans. Energy Convers.*, vol. 20, no. 2, pp. 381–387, Jun. 2005.

[30] J. Padulles, G. W. Ault, and J. R. McDonald, "An integrated SOFC plant dynamic model for power systems simulation," *J. Power Sources*, vol. 86, nos. 1–2, pp. 495–500, Mar. 2000.

[31] CIGRE. (May 15, 2013). *Benchmark Systems for Network Integration of Renewable and Distributed Resources*. [Online]. Available: http://www.e-cigre.org/Order/select.asp?ID=16639

[32] R. Melloni, "A multi-site European network for real-time co-simulation of transmission and distribution systems," Ph.D. dissertation, Dept. Energy, Politecnico di Torino, Turin, Italy, 2017.

[33] Z. Li, J. Wang, H. Sun, and Q. Guo, "Transmission contingency analysis based on integrated transmission and distribution power flow in smart grid," *IEEE Trans. Power Syst.*, vol. 30, no. 6, pp. 3356–3367, Nov. 2015.

[34] C. S. Edrington, M. Steurer, J. Langston, T. E. Mezyani, and K. Schoder, "Characteristics and design of power hardware-in-the-loop simulations for electrical power systems," *IEEE Trans. Ind. Electron.*, vol. 63, no. 1, pp. 406–417, Jan. 2016.

[35] E. M. Stewart, R. Tumilty, J. Fletcher, A. Lutz, G. Ault, and J. McDonald, "Analysis of a distributed grid-connected fuel cell during fault conditions," *IEEE Trans. Power Syst.*, vol. 25, no. 1, pp. 497–505, Feb. 2010.

**ABOUZAR ESTEBSARI** (Senior Member, IEEE) received the Ph.D. degree in electrical engineering from the Politecnico di Torino, Italy, in 2015. He was a Postdoctoral Research Fellow with the Politecnico di Torino, from 2015 to 2017. In 2016, he was with RWTH-Aachen University, Germany, as a Visiting Scholar. From 2017 to 2020, he was an Assistant Professor in electrical engineering with the Politecnico di Torino. In 2019, he was a Research Scholar with the Department of Electrical and Computer Engineering, The George Washington University, Washington, DC, USA. In 2020, he joined London South Bank University, U.K., where he is currently an Associate Professor in electrical engineering. He has authored or coauthored more than 60 peer-reviewed papers published in international journals and in the proceedings of international conferences. His research interests include power system security of supply and resiliency, smart grid applications, multi-vector energy systems, and power system simulations.

He was a recipient of the Manby Prize ICT/GIS/BIM 2020 of ICE in the U.K.

**STEFFEN VOGEL** (Student Member, IEEE) is currently pursuing the Ph.D. degree with the Institute for Automation of Complex Power Systems under the supervision of Prof. Monti. He is also a Research Associate with the Institute for Automation of Complex Power Systems under the supervision of Prof. Monti. He studied computer engineering at RWTH Aachen and he is currently working in the field of real-time systems and geographically distributed real-time simulation. He is also the Lead-Developer of VILLASframework, a toolkit for distributed real-time simulation.

**RENATO MELLONI** was born in Bolzano, Italy, in 1992. He received the M.Sc. degree in electrical engineering from the Polytechnic University of Turin, Italy, in 2017.

He has worked at Fri-El Green Power and Lightsource bp as a Grid Connection Specialist for utility-scale wind and PV plants and is currently the Project Manager at CIC Energy.

**MARIJA STEVIC** received the B.Sc. and M.Sc. degrees in electrical engineering from the University of Belgrade, Serbia, in 2009 and 2012, respectively.

She was with the Institute for Automation of Complex Power Systems, RWTH Aachen University, Germany, from 2012 to 2020. In 2016 and 2017, she was a Visiting Researcher with the Idaho National Laboratory, USA. In 2020, she joined OPAL-RT Germany GmbH as a Research and Development Engineer. Her research interests include distributed real-time simulation, real-time simulation of power electronics applications, and hardware-in-the-loop.

**ETTORE F. BOMPARD** (Member, IEEE) is currently a Professor in power systems with the Politecnico di Torino (Polito, present), a Senior Scientist at the Joint Research Center of the European Commission, Energy Systems, Security and Market Unit, Institute for Energy and Transport, from 2012 to 2014, and a Visiting Assistant Professor with the Electrical and Computer Engineering Department, University of Illinois at Urbana–Champaign, USA, with a Fulbright Scholarship, in 2000. He is also a Scientific Advisor as an Expert, for Directorate B "Growth & Innovation" and Directorate C "Energy Transport & Climate" of the DG Joint Research Center of the European Commission. Scientific director of the ESTLab@EnergyCenter (Energy Security and Transition Laboratory). He has been the Scientific Coordinator of many research projects in the framework of the Italian System Research on Power Systems, EU-funded projects, Next Generation Infrastructure (The Netherlands), and NATO Projects. He is the coauthor of more than 150 publications.

**ANTONELLO MONTI** (Senior Member, IEEE) received the M.Sc. *(summa cum laude)* and Ph.D. degrees in electrical engineering from the Politecnico di Milano, Milan, Italy, in 1989 and 1994, respectively. He started his career with Ansaldo Industria and then moved, in 1995, to the Politecnico di Milano as an Assistant Professor. In 2000, he joined the Department of Electrical Engineering, University of South Carolina, Columbia, SC, USA, as an Associate Professor and later became a Full Professor. Since 2008, he has been the Director of the Institute for Automation of Complex Power System, E.ON Energy Research Center, RWTH Aachen University, Aachen, Germany. Since 2019, he also has a joined appointment at Fraunhofer FIT within the Center for Digital Energy Aachen. He has authored or coauthored more than 400 peer-reviewed papers published in international journals and in the proceedings of international conferences. He is an Associate Editor for *IEEE Electrification Magazine*. He is a member of the Editorial Board of the *Sustainable Energy, Grids and Networks* and a the Founding Board of the *Energy Informatics*. He was a recipient of the 2017 IEEE Innovation in Societal Infrastructure Award.

● ● ●